Unusual bismuth-containing surface layers of III-V compound semiconductors

by Marja Ahola-Tuomi

TURUN YLIOPISTO

Turku 2013

From the Department of Physics and Astronomy

University of Turku

Turku, Finland

and

Graduate School of Materials Research (GSMR)

Turku, Finland

Supervised by

Docent Pekka Laukkanen

Docent Marko Punkkinen

Emeritus Professor Juhani Väyrynen

University of Turku

Turku, Finland

Reviewed by

Professor Marko Huttula

University of Oulu

Docent Mika Hirsimäki

Tampere University of Technology

Contents

Acknowledgements **1**

Abstract **2**

List of papers **3**

1 Introduction **7**

1.1 III-V semiconductor technology 7

1.2 Role of bismuth-containing surface layers in technology 8

2 Properties of III-V(100) semiconductor surfaces **11**

2.1 Electronic structure of III-V semiconductors 12

2.2 Formation of III-V(100) surface: electron counting rule 14

2.2.1 Reconstructions of III-V(100) surface 16

2.2.2 Violations of the electron counting rule 17

3 Surface characterization techniques **19**

3.1 Low energy electron diffraction (LEED) 20

3.2 Scanning tunneling microscopy (STM) 22

3.2.1 Imaging the III-V(100) semiconductor surface 24

3.3 Photoelectron spectroscopy 25

3.3.1 Synchrotron radiation photoelectron spectroscopy 28

3.3.2 The interpretation of the spectra 31

3.4 Sample preparation 33

4 Results and discussion **35**

4.1 Bi-stabilized (2×4) reconstruction on III-V(100) semiconductor surfaces 36

4.2 Unusual (2×1) reconstruction on III-V(100) surface 38

4.3 Formation of Bi nanolines on InAs(100) surface 40

5 Conclusions **43**

References **44**

Original papers **48**

Acknowledgements

I am sincerely and heartily grateful to my supervisors Pekka Laukkanen and Marko Punkkinen. Without Pekka, my dissertation would have never been completed. Without Marko's theoretical counterpart, the papers would have never reached their scientific value. I would like to thank both for being my friends and supporting me also through the times I wasn't working full time with my thesis. I owe sincere thankfulness to my professor, Juhani Väyrynen, for the guidance during the first years of my postgraduate studies. It is a great pleasure to thank all my colleagues and friends in our laboratory of Materials Research and the Department of Physics and Astronomy, who helped me with the measurements and helped me to write my dissertation successfully. Special thanks to Karina Schulte for introducing me to the exiting world of synchrotrons. Also, I cannot emphasize enough of the value of her moral support.

I would like to acknowledge the institutions and research groups I have collaborated internationally: MAX-laboratory and its staff in Lund, Sweden. ISA and Department of Physics and Astronomy, especially the surface science group led by Professor Philip Hofmann in Aarhus, Denmark. Nottingham Nanoscience group led by Professor Philip Moriarty in England.

I am truly indebted and thankful to Mikko Tuomi for his support throughout my thesis writing. Finally, I would like to acknowledge the funding from the Graduate School of Materials Research, a Framework 6 Early Stage Training Network NANOCAGE, and Finnish Cultural Foundation.

Marja Ahola Tuomi

Turku, May 2013

Abstract

The understanding and engineering of bismuth (Bi) containing semiconductor surfaces are significant in the development of novel semiconductor materials for electronic and optoelectronic devices such as high-efficiency solar cells, lasers and light emitting diodes. For example, a Bi surface layer can be used as a surfactant which floats on a III-V compound-semiconductor surface during the epitaxial growth of III-V films. This Bi surfactant layer improves the film-growth conditions if compared to the growth without the Bi layer. Therefore, detailed knowledge of the properties of the Bi/III-V surfaces is needed. In this thesis, well-defined surface layers containing Bi have been produced on various III-V semiconductor substrates. The properties of these Bi-induced surfaces have been measured by low-energy electron diffraction (LEED), scanning-tunneling microscopy and spectroscopy (STM), and synchrotron-radiation photoelectron spectroscopy. The experimental results have been compared with theoretically calculated results to resolve the atomic structures of the studied surfaces. The main findings of this research concern the determination of the properties of an unusual Bi-containing (2×1) surface structure, the discovery and characterization of a uniform pattern of Bi nanolines, and the optimization of the preparation conditions for this Bi-nanoline pattern.

List of papers

1. P. Laukkanen, **M. Ahola**, M. Kuzmin, R. E. Perälä and I. J. Väyrynen: *Bi-induced (2×6), (2×8) and (2×4) reconstructions on InAs(100) surface*, Surface Science Letters 598 (2005) L361.

2. **M. Ahola-Tuomi**, P. Laukkanen, R. E. Perälä, M. Kuzmin, J. Pakarinen, I. J. Väyrynen, and M. Adell: *Structural properties of Bi-terminated GaAs(001) surface*, Surface Science 600 (2006) 2349.

3. P. Laukkanen, **M. Ahola-Tuomi**, M. Kuzmin, R. E. Perälä, I. J. Väyrynen, A. Tukiainen, J. Pakarinen, M. Saarinen, and M. Pessa: *Structural properties of Bi-stabilized reconstructions of GaInAs(100) surface*, Applied Physics Letters 90 (2007) 082101.

4. P. Laukkanen, M. P. J. Punkkinen, H.-P. Komsa, **M. Ahola-Tuomi**, K. Kokko, M. Kuzmin, J. Adell, J. Sadowski, R. E. Perälä, M. Ropo, T. T. Rantala, I. J. Väyrynen, M. Pessa , L. Vitos, J. Kollár, S. Mirbt, and B. Johansson: *Anomalous bismuth-stabilized (2×1) reconstructions on GaAs(100) and InP(100) surfaces*, Physical Review Letters 100 (2008) 086101.

5. M. P. J. Punkkinen, P. Laukkanen, H.-P. Komsa, **M. Ahola-Tuomi**, N. Räsänen, K. Kokko, M. Kuzmin, J. Adell, J. Sadowski, R.E. Perälä, M. Ropo, A. Tukiainen, T.T. Rantala, I.J. Väyrynen, M. Pessa, L. Vitos, J. Kollár, S. Mirbt, and B. Johansson: *Bismuth-stabilized (2×1) and (2×4) reconstructions on the III-V(100) surfaces: A combined first-principles and photoemission and scanning-tunneling-microscopy study*, Physical Review B 78 (2008) 195304.

6. **M. Ahola-Tuomi**, P. Laukkanen, M. P. J. Punkkinen, M. Kuzmin, R. E. Perälä, I. J. Väyrynen, K. Schulte and M. Pessa: *Formation of an ordered pattern of Bi nanolines on InAs(100) by self-assembly*, Applied Physics Letters

92 (2008) 011926.

7. **M. Ahola-Tuomi**, M. P. J. Punkkinen, P. Laukkanen, M. Kuzmin, J. Lång, K. Schulte, N. Räsänen, R. E. Perälä, and I. J. Väyrynen: *Properties of self-assembled Bi nanolines on InAs(100) studied by core-level and valence-band photoemission and first-principles calculations*, Physical Review B 83 (2011) 245401.

The following papers are closely related to this work but not included in the thesis.

- P. Laukkanen, M.P.J. Punkkinen, N. Räsänen, **M. Ahola-Tuomi**, J. Sadowski, J. Adell, M. Kuzmin, J. Lång, R.E. Perälä, M. Ropo, K. Kokko, L. Vitos, B. Johansson, M. Pessa, and I.J. Väyrynen: Bismuth-stabilized c(2x6) reconstruction on InSb(100) substrate: Violation of the electron counting model, Physical Review B 81 (2010) 035310.

- R. E. Perälä, M. Kuzmin, P. Laukkanen, **M. Ahola-Tuomi**, M. P. J. Punkkinen, and I.J. Väyrynen: Ytterbium on vicinal Si(100): Growth and properties of the 2D wetting layer and the Yb silicide phase, Surface Science 603 (2009) 102.

- M.P.J. Punkkinen, P. Laukkanen, **M. Ahola-Tuomi**, J. Pakarinen, M. Kuzmin, A. Tukiainen, R.E. Perälä, J. Lång, M. Ropo, K. Kokko, L. Vitos, B. Johansson, M. Pessa, I.J. Väyrynen: Core-level shifts of InP(100)(2×4) surface: Theory and experiment, Surface Science 603 (2009) 2664.

- M. P. J. Punkkinen, P. Laukkanen, H.-P. Komsa, **M. Ahola-Tuomi**, N. Räsänen, K. Kokko, M. Kuzmin, J. Adell, J. Sadowski, R. E. Perälä, M. Ropo, T. T. Rantala, I. J. Väyrynen, M. Pessa, L. Vitos, J. Kollár, S. Mirbt, and B. Johansson: Bismuth-stabilized (2×1) and (2×4) reconstructions on GaAs(100) surfaces: Combined first-principles, photoemission, and scanning tunneling microscopy study, Physical Review B 78 (2008) 195304.

- M. Kuzmin, M. P. J. Punkkinen, P. Laukkanen, R. E. Perälä, **M. Ahola-Tuomi**, T. Balasubramanian, and I. J. Väyrynen: Yb-induced (2×3) and (2×4) reconstructions on Si(100) studied by first-principles calculations and high-resolution core-level photoelectron spectroscopy, Physical Review B 78 (2008) 045318.

- M. P. J. Punkkinen, K. Kokko, L. Vitos, P. Laukkanen, E. Airiskallio, M. Ropo, **M. Ahola-Tuomi**, M. Kuzmin, I. J. Väyrynen, and B. Johansson: Calculation of surface core-level shifts within complete screening: Problems with pseudohydrogenated slabs, Physical Review B 77 (2008) 245302.

- P. Laukkanen, **M. Ahola-Tuomi**, J. Adell, M. Adell, K. Schulte, M. Kuzmin, M. P. J Punkkinen, J. Pakarinen, A. Tukiainen, R. E. Perälä, I. J. Väyrynen and M. Pessa: A comparative study of clean and Bi-stabilized InP(100)(2×4) surfaces by core-level photoelectron spectroscopy, Surface Science 601 (2007) 3395.

- M. P. J. Punkkinen, P. Laukkanen, K. Kokko, M. Ropo, **M. Ahola-Tuomi,** I. J. Väyrynen, H.-P. Komsa, T. T. Rantala, M. Pessa, M. Kuzmin, L. Vitos, J. Kollár and B. Johansson: Surface core-level shifts of GaAs(2×4) from first principles, Physical Review B 76 (2007) 115334.

- M. Kuzmin, K. Schulte, P. Laukkanen, **M. Ahola-Tuomi**, R. E. Perälä, M. Adell, T. Balasubramarian and I. J. Väyrynen: Atomic and Electronic structure of the Yb/Ge(111)-(3×2) surface studied by high-resolution photoelectron spectroscopy, Physical Review B 75 (2007) 165305.

- M. Kuzmin, P. Laukkanen, R. E. Perälä, **M. Ahola-Tuomi** and I. J. Väyrynen: High-resolution core-level photoemission study of Ge(111)2×1-Sb and Ge(111)($\sqrt{3} \times \sqrt{3}$)R30°-Bi reconstructions, Journal of Electron Spectroscopy 159 (2007) 24.

- M. Kuzmin, P. Laukkanen, R.E. Perälä, **M. Ahola-Tuomi** and I.J. Väyrynen: Atomic geometry and electronic properties of the Ge(111)(2×1)-Sb surface studied by scanning tunneling microscopy/spectroscopy and core-level photoemission, Surface Science 601 (2007) 873.
- P. Laukkanen , J. Pakarinen, **M. Ahola-Tuomi**, M. Kuzmin, R. E. Perälä, I. J. Väyrynen, A. Tukiainen, J. Konttinen, V. Rimpiläinen, and M. Pessa: Structural and electronic properties of Bi-adsorbate-stabilized reconstructions on the InP(100) and GaAsN(100) surfaces, Physical Review B 74 (2006) 155302.
- M. Kuzmin, R. E. Perälä, P. Laukkanen, **M. Ahola-Tuomi**, and I. J. Väyrynen: High-resolution core-level photoemission study of Eu-induced (3×2)/(3×4) reconstruction on Ge(111), Physical Review B 74 (2006) 115320.
- P. Laukkanen, J. Pakarinen, **M. Ahola-Tuomi**, M. Kuzmin, R. E. Perälä, I. J. Väyrynen, A. Tukiainen, V. Rimpiläinen, M. Pessa, M. Adell, and J. Sadowski: Electronic and structural properties of the InP(100)(2×4) surface studied by core-level photoemission and scanning tunneling microscopy, Surface Science 600 (2006) 3022.
- P. Laukkanen, M. Kuzmin, R. E. Perälä, **M. Ahola**, S. Mattila, I. J. Väyrynen, J. Sadowski, J. Konttinen, T. Jouhti, C. Peng, M. Saarinen, and M. Pessa: Electronic and structural properties of GaAs(100)(2×4) and InAs(100)(2×4) surfaces studied by core-level photoemission and scanning tunneling microscopy, Physical Review B 72 (2005) 045321.

In Addition, other work related to the surface studies of nanostructures have been carried out internationally.

- F. Song, J. W. Wells, K. Handrup, Z. S. Li, S. N. Bao, K. Schulte, **M. Ahola-Tuomi**, L. C. Mayor, J. C. Swarbrick, E. W. Perkins, L. Gammelgaard, and Ph. Hofmann: Direct measurement of electrical conductance through a self-assembled molecular layer, Nature Nanotechnology 4 (2009) 373.
- K. Schulte, C. Yan, **M. Ahola-Tuomi**, A. Stróżecka, P. J. Moriarty and A. Khlobystov: Encapsulation of CoPc molecules in carbon nanotubes, Journal of Physics: Conference series 100 (2008) 012017.
- P. Moriarty, M. Blunt, C. Martin, **M. Ahola-Tuomi**, E. Pauliac-Vaujour, P. Sharp, P. Nativo, and M Brust: Coerced Coarsening of Nanoparticle Assemblies: A Mechanical Drive Towards Equilibrium, Nature Nanotechnology 2 (2007) L167.

1 Introduction

1.1 III-V semiconductor technology

Since the invention of a bipolar transistor in 1947 by Bardeen and Brattain, which was the first observation of an amplification of the input signal in a point contact, the semiconductor industry has exploded into a largest industry in the world: the electronic industry. The electronic devices are largely based on silicon (Si), which is relatively inexpensive and easily available, but it has its limitations. According to the Moore's law, the number of transistors that can fit on an integrated circuit doubles every two years, which means that components become smaller and devices more powerful. If the size of a Si-transistor is further decreased, some serious disadvantages will soon become evident. For example, the leakage currents increase so more power is consumed and more heat is generated. Also, silicon has very low efficiency in light generation due to its indirect bandgap [1]. To take advantage of the silicon technology infrastructure, but add new electric and especially optoelectronic properties to the components, the integration of III-V semiconductor films, such as gallium phosphide (GaP), gallium arsenide (GaAs), indium phosphide (InP), and indium arsenide (InAs) on silicon substrates is under extensive study. This is needed to produce new, high-performance materials for semiconductor industry. [2].

Semiconductor devices consist of layers of different semiconductor materials. These film stacks are usually produced by growth techniques such as molecular beam epitaxy (MBE) and metal organic chemical vapor deposition (MOCVD). In these processes, layers of different type of semiconductor films are grown by one atomic layer over another until the desired thickness is reached. The basic goal of the research and the development of semiconductor materials is to improve the crystal quality. Nobel laureate Herbert Kroemer has described the importance of device interfaces as follows: "Often, it may be said that the interface is the device".

Thus, the interfaces between different types of semiconductors have a crucial role in the operation of devices like laser diode and solar cell, and the role of the interface increases in the future because the physical size of devices is reduced.

In the MBE chamber, it is possible to monitor the crystal structure and quality of film during the film growth in real time. The epitaxial growth is essentially a surface process which is governed by the atomic and electronic structure of a semiconductor surface. Usually a clean semiconductor surface is reconstructed; its atomic structure is clearly different from that of the corresponding plane in the bulk, as described later. Thus, the growth front of a film or a stack of films is often reconstructed during the whole growth process. A surface reconstruction can change during the growth, and it is of great importance to know the properties of the surface in order to optimize the parameters for the best quality interface - the best quality devices. In this thesis, technologically relevant III-V compound semiconductor surfaces are studied. The research focuses on the III-V(100) surface, which usually serves as a substrate for epitaxial growth.

1.2 Role of bismuth-containing surface layers in technology

There is substantial interest in developing new classes of semiconductor materials exploiting the properties of a group V semimetal bismuth. These include materials for development of optoelectronic, thermoelectric and electronic devices such as laser diodes (used for optical communications, DVD systems etc.), light emitting diodes and solar cells [3–8]. On the other hand, bismuth is a striking example of the possible difference between surface and bulk material properties. Bi surfaces are much better conductors than bulk, but thin films of Bi with thickness of less than about 35 nm have a semiconducting character [9]. Thus, there is a delicate balance of Bi being either a metal or a semiconductor. Also, a strong spin-orbit interaction leads to a splitting of the surface state bands with respect to their spin direction. Thus, Bi

surfaces or nanostructures could be used as spin-selectors in electronic devices (i.e. spintronics) [5, 9].

The growth of a rather new III-V compound, $GaAs_{1-x}Bi_x$ is one example why integration of Bi into III-V compound semiconductors has become an interesting topic in research [6]. It has been found that a low growth temperature (less than 400 °C) is needed to incorporate Bi into the crystal, which means that Bi atoms only float in the growth front at the normal growth temperatures (500-650 °C) of III-V films, and will not be incorporated into the lattice. This property makes Bi a potential surfactant, which means that using Bi during the film growth, the quality of the III-V semiconductor film is improved [7]. In particular, it has been considered that Bi-surfactant improves the crystal quality of III-V films which must be grown at low temperatures. This is related to a Bi-induced change in the atomic structure of the surface. It is yet unclear, which surface structure is the best for producing well-ordered and smooth interfaces. This makes the Bi/III-V(100) surface a relevant subject to study, since hardly any research has been done on Bi/III-V(100) surfaces previously.

In this thesis, a number of Bi/III-V(100) surface structures have been investigated. Papers 1-3 consider the Bi-stabilized surface structures that are common for the III-V(100)surfaces. A newly found Bi/GaAs(100)(2×1) surface structures is discussed in the papers 4 an 5. Also, a very recent study of M. Masnadi-Shirazi et al. [12] demonstrated that this Bi-induced (2×1) reconstruction, which is not normally seen during the III-V epitaxy, is a very useful surface for the growth of $GaAs_{1-x}Bi_x$ films. If compared to other reconstructions observed during the $GaAs_{1-x}Bi_x$ growth, this unusual (2×1)-Bi surface provides a clear improvement in the Bi incorporation into the crystal, and also better photoluminescence intensity of the grown film.

From another technological point of view, formation of periodically ordered nanoscale structures offers a possibility to fabricate prototype electronic devices

based on the quantum confinement of electron states. Semiconductor surfaces are particularly interesting in this aspect since the surface states inside the gap cannot couple with the substrate [13]. Furthermore, different nanostructures can be used as templates to grow other ordered nanoscale systems. Besides the fundamental studies of exotic behavior of quantized electronic states and charge transport, such structures could be used, for example, as interconnections in nanoelectronics [13,14]. Different nanowires have been extensively studied on silicon with some remarkable results [13–17]. In contrast, only a few studies have been reported on 1D systems on III-V(100) semiconductor surfaces which is surprising considering their technological importance. Besides the study of the Bi/III-V(100) interface and the unusual Bi-induced (2×1) surface reconstruction, it is also shown in this thesis that it is possible to create a large-scale, single-domain pattern of nanolines on the Bi/InAs(100)(2×1) substrate. The structural properties of these Bi nanolines are studied in the papers 6 and 7.

2 Properties of III-V(100) semiconductor surfaces

Most semiconductors studied or used in technology are single crystals, which means that they have a well-defined crystalline structure. Compared to bulk, surfaces and interfaces are usually composed of atoms which do not have a full complement of neighbours. An ideal single crystal surface is defined by Miller indices, which have a simple meaning in the case of a cubic crystal [18]. The symbol (100), for example, denotes surfaces perpendicular to the cubic x-axis. The (100) surface and the planes physically equivalent to it are shown in Fig. 1a. The creation of a surface or an interface requires an input of energy, the surface free energy. In the bulk of any material, cohesive interactions of neighbouring atoms hold them together. Since a surface atom has fewer neighbours, a significant rebonding of surface atoms occurs on many semiconductors surfaces. This leads to a numerous different processes taking place on the surface, resulting in surface behaviour which can be completely different from that of a bulk crystal.

One of the processes, which reduces the surface free energy, is called *surface relaxation*. It is a process leading to a compression or expansion of the interplanar atomic distances of the surface layers in the surface normal direction. In the surface relaxation, the crystal lattice of a surface layer does not change. *Surface reconstruction* is more complicated phenomenon in which atomic rearrangements introduce a lateral change in the surface periodicity (i.e. the change in the surface lattice structure), which happens simultaneously with surface relaxation. The study of III-V compound semiconductor surfaces (of which the (100) surface being the most important in technology), a number of different surface structures with different properties have been found over the last decades on III-V(100) surfaces [21–27, 29–31] The reconstruction that appears in reality depends strongly on the preparation conditions of the III-V surface in question. Also adsorbates like antimony (Sb) has been found to induce reconstructions on III-V(100) surfaces [23, 28, 32]. An adsorption of another

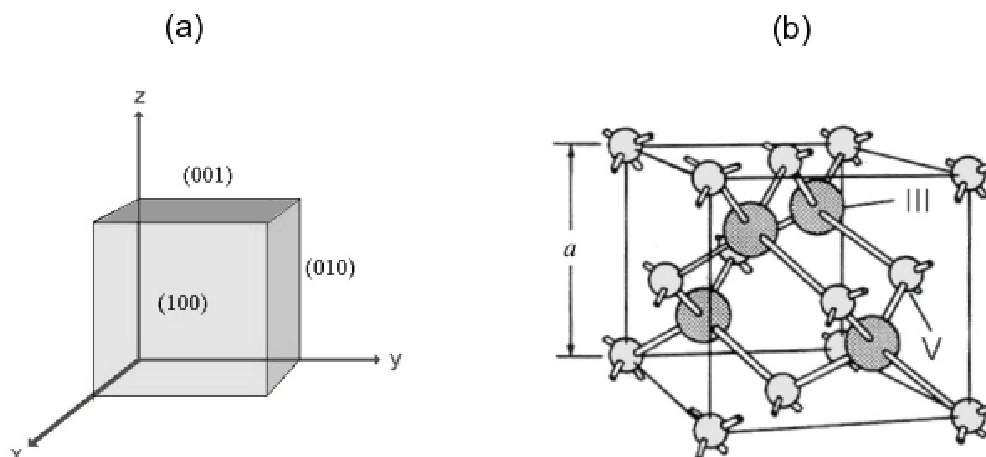

Figure 1. a) Planes physically equivalent to the (100) plane in a cubic crystal. b) Zincblende unit cell for III-V semiconductors and lattice parameter a [1].

group V element, bismuth (Bi), have been investigated in this thesis, since to a large extent, Bi-induced surface structures on III-V compound semiconductors have been an unexplored field.

2.1 Electronic structure of III-V semiconductors

The elemental semiconductors have a diamond lattice structure, in which each atom is bonded to four neighbours which lie in the corners of a tetrahedron. Most of the III-V compound semiconductors have a zincblende structure, which is identical to the diamond lattice but in the zincblende structure each atom's nearest neighbors are of the opposite type. This is shown in Fig 1b. The bond between two nearest neighbours can be described with sp^3 hybrid orbitals including two electrons with opposite spins. Hybridization is a concept of mixing atomic orbitals to form new hybrid orbitals. The names of the new hybrid orbitals are based on the atomic orbitals involved in the hybridization. In III-V semiconductors, s^2p^1 electrons of group III atoms and s^2p^3 electrons of group V atoms form the sp^3 hybrid bonds which define the zincblende lattice structure with tetrahedral bonding [1].

Atoms in III-V zincblende lattice share their valence electrons with their four neighbouring atoms. An individual atom has discrete energy levels. With a reduction in the interatomic spacing, these valence energy levels merge into an energy band of a semiconductor. As the interatomic spacing approaches the equilibrium spacing of the crystal, the overlapping hybrid orbitals corresponds to the formation of bonding and antibonding molecular orbitals. The energy band splits into two bands separated by an energy gap E_g, where no allowed energy states for electrons exist. The lower energy band or valence band corresponds to bonding, and the higher energy band or conduction band corresponds to anti-bonding levels [1, 33]. This is obviously a simplified interpretation of a 'real life' crystal, in which the resulting band structure is generally quite complex and may have mixed bonding and anti-bonding character when all relevant atomic orbitals are overlapped.

The position of the Fermi level is a relevant characteristic to understand various devices. The Fermi energy is defined as the highest occupied energy level at the temperature $T = 0$ K. At elevated temperatures, the highest occupied energy level cannot be defined since there are electrons constantly excited in the bands. The Fermi-Dirac distribution gives the probability that an electron will occupy a state having energy E [18,33]. In semiconductors, *the Fermi level* E_F (or chemical potential) is defined as the energy state where the Fermi distribution function equals 0,5 at $T \neq 0$. In other words, the Fermi level is the energy level with 50 % change of being occupied by an electron. The lowest energy level is called the *vacuum level*. This is assumed to be zero and outside of the crystal. The *work function* Φ is the minimum amount of energy needed to remove an electron from the solid. Thus, the value of Φ is the difference in energy between the vacuum level and Fermi level E_F [18].

In an intrinsic semiconductor, the Fermi level locates in the middle of the band gap E_g. If the material is n-doped (extra electrons are added), the Fermi level

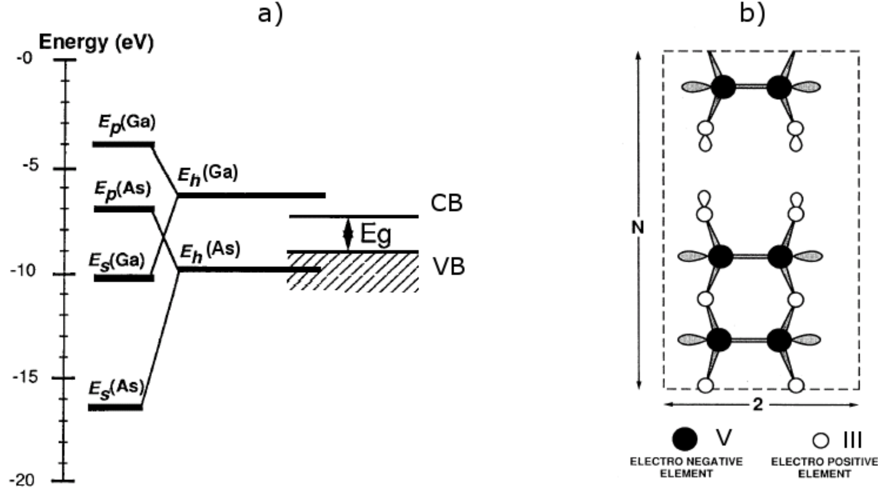

Figure 2. a) The energy level diagram for the III-V compound semiconductor surface. E_g denotes the band gap, and CB and VB are the conduction band minimum and valence band maximum, respectively. The data are from W. A. Harrison, ref. [20] b) The (2×4) unit cell. The image is reprinted from M. D. Pashley, ref. [21].

moves closer to the conduction band, and vice versa in the p-doped material. A good question is how the Fermi-level position can be determined because there are usually no electron states in the band gap. Experimentally, photoelectron spectroscopy provides an elegant solution to the question [18].

2.2 Formation of III-V(100) surface: electron counting rule

The atoms in the III-V compound semiconductors are bonded to each other with sp^3 hybridized electron orbitals. When a surface is formed, these bonds break and leave partially filled sp^3 hybrid orbitals. These half-filled surface bonds are called *dangling bonds* and are energetically significantly unfavoured, because attractive electron – ion interactions are not efficiently exploited by broken bonds. This leads to formation of surface dimer bonds, which means that the surface atoms couple to reduce the number of dangling bonds. Generally, the dimer atoms can be similar (homodimer) or different (heterodimer), although homodimers are more common.

The energy levels of these hybrid (dangling) bond states (E_h) can be estimated

from the energies of the s and p atomic energy levels (E_s and E_p) they are derived from. The energy levels are shown schematically in Fig. 2a [20, 21]. The dangling-bond energy of the electropositive element (group III) is in the conduction band and therefore should be empty, and the dangling-bond energy of the electronegative element (group V) is in the valence band and should be filled. This is the physical ground for the so-called electron counting rule (or electron counting model), which describes a sufficient condition for the formation of a semiconducting surface. If the energy levels of the group III and group V dangling bonds would be close to each other, the electron counting rule would not be satisfied.

The electron counting rule requires that a surface structure is found where the number of available electrons in the surface layer(s) fill all the dangling bonds of the group V elements leaving all the dangling bonds of group III elements empty [21]. One should, however, keep in mind that the concept of a dangling bond is a simplification, because the dangling bond charge distribution is rather similar to charge distributions of other bonds. Also, all valence charge is delocalized characteristic of periodic solid state systems. It is essential that the energy bands associated to dangling bonds comply with the electron counting rule. This happens because the energy levels of the atomic hybrid orbitals are far enough from each other.

Due to the surface dimer formation, a $2\times$ periodicity in the [110] direction is found on the surface [21]. However, the resulting surface becomes energetically unstable unless some amount of the dimers is removed from the surface [22]. The $N\times$ periodicity arises from these missing dimers. According to the electron counting rule, the smallest unit cell which satisfies these conditions is a (2×4) unit cell, where every fourth dimer is missing. An example of this is shown in Fig. 2b [21].

2.2.1 Reconstructions of III-V(100) surface

A semiconducting surface reconstruction on III-V(100) surface requires enough electrons to fill the dimer bonds and the dangling bonds that locate below the Fermi level. Also, electrons are needed to bond the surface dimers to the subsurface layer(s). On the other hand, the subsurface layers can also be involved in the reconstructions, which leads to a number of possible different atomic structures, which satisfy the conditions of the electron counting rule. Extensive experimental and theoretical research has been conducted in order to find energetically most favoured structures on various III-V(100) compound semiconductor surfaces [21–32, 37]. For example, on GaAs(100) which is probably the most studied one of the III-V semiconductor surfaces, the periodicity or reconstruction changes from the most As-rich c(4×4) via (2×4) to the Ga-rich (4×2) as the temperature of the sample increases from 300 °C to about 650 °C, until Ga starts to form metallic droplets before the crystal decomposes. A summary of these reconstructions and their different *phases*, i.e. different atomic structures with the same symmetry, are discussed in more detail in Refs. [24, 25, 29], for example.

According to the basic principles, the (2×4) reconstruction is the smallest energetically favoured semiconducting structure on III-V(100) surfaces. This is also the most commonly used substrate during the MBE-growth of films for electronic devices. The exact atomic structure for this reconstruction has been under debate for a number of decades [21, 23–25, 30]. As an example, two different atomic structures called $\alpha 2$ and $\beta 2$ are shown in Fig. 3 for the III-V(100)(2×4) reconstruction. They both are found to be stable and semiconducting. Both structures are group V stabilized, but $\alpha 2$ dominates in slightly less group V-rich conditions. Besides GaAs(100), InAs(100) goes through similar phase transitions from the As-rich (2×4) to In-rich (4×2) surface reconstruction, but at somewhat lower temperatures. The atomic geometry of the InAs(100) and GaAs(100) (2×4) surfaces are almost identical [27].

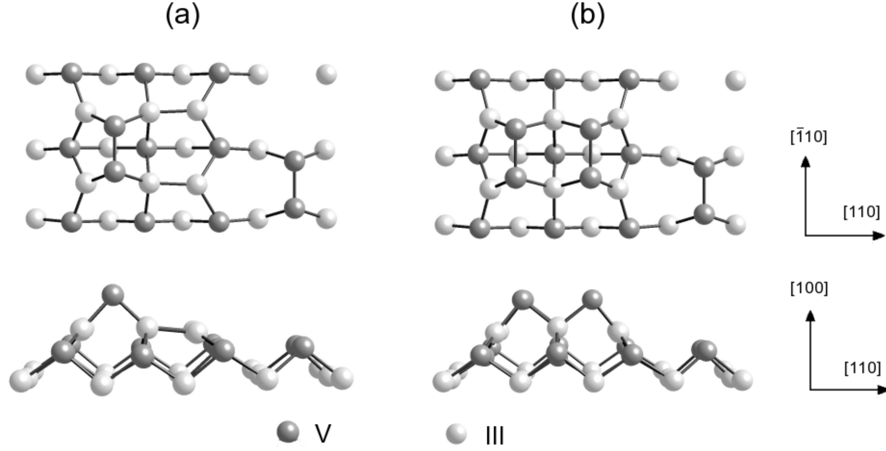

Figure 3. The top and side view of two different atomic structures, called $\alpha 2$ (a) and $\beta 2$ (b) phase for the III-V(100)(2×4) reconstruction. The $\alpha 2$ has one top group V dimer and the $\beta 2$ has two group V dimers on the top surface layer, and both have one top group V dimer in the third layer.

Also, the InP(100) surface has the (2×4) periodicity, but the atomic model is slightly different, including mixed In-P dimers on the surface layer(s) [28, 37].

2.2.2 Violations of the electron counting rule

In general, most of the III-V(100) surface reconstructions obey the basic principles established for III-V semiconductors. However, there are findings of surface structures that appear to be stable, but still violates the electron counting rule. For example, for the GaSb(100) surface a stable, weakly metallic (1×3) reconstruction among some other metallic GaSb(100) reconstructions have been reported [38, 39]. Midgap conductivity is observed on these GaSb(100) surfaces as a direct consequence of the violation of the electron counting rule [38]. The reason for this is suggested to be related to the substantial amount of atomic relaxation (increase of the vertical distance of the surface atomic layers compared to bulk) taking place on the GaSb(100) surface due to the large bond length of Sb atoms, which helps to stabilize these structures [39].

Another surface worth mentioning is a stable, semiconducting InP(100)(2×1)

reconstruction, which has been studied both experimentally and theoretically [40]. Such a small surface unit cell should include a half-filled dangling bond and without any dimer vacancies, the surface should be metallic and unstable. After a number of years of research, however, this InP(100)(2×1) was found to be stabilized by hydrogen, which is present during the metal organic vapor phase epitaxy (MOVPE) growth of the InP(100) samples [41]. Furthermore, hydrogen is almost impossible to detect by experimental methods such as STM and photoemission. This is a good example of the need to be extremely careful in interpretation of the data and include complementary experimental and theoretical methods to find the correct answers for these problems. As described above, the most of III-V surface structures found obey the electron counting rule. However, another remarkable exception has been found and described in this thesis, and since only a handful of these peculiar surface structures have truly been found, it is of great challenge to study these systems.

3 Surface characterization techniques

Surface science deals often with well-defined surfaces from the viewpoint of their structure and composition. These surfaces are either adsorbate-free and clean on the atomic level, or adsorbate-covered, containing a certain species of adsorbates, which have been added in a precisely controlled manner. This is possible only under ultra high vacuum (UHV) conditions with the base pressure better than 1^{-10} mbar. In the research presented in this thesis, different surface characterization techniques have been used in the UHV system in our Laboratory of Materials Research in University of Turku. Also, experiments have been performed at synchrotron radiation facilities in MAX-Laboratory in Lund, Sweden, and at ISA - Centre for Storage Ring Facilities in Aarhus, Denmark. From the experimental point of view, it is important to use several experimental methods to get a comprehensive view of the surface under study, since every method has its advantages as well as limitations. The experimental research in this thesis is mainly a combination of three different measuring techniques; *Low energy electron diffraction* (LEED), which is used as an initiative method to evaluate the surface quality on a large scale. Secondly, *Scanning tunneling microscopy* (STM) is utilized to obtain an image of the surface in nanoscale range. Last but not least, *synchrotron radiation photoemission spectroscopy* gives information of the chemical environment of the surface atoms which complements the atomic structure derived from the STM images.

Also, the experimental results have been combined with theoretical calculations, which were performed using the *ab initio* density-functional total energy code with the local density approximation [34, 35] to improve the physical understanding of the observations. The method of calculations is described elsewhere [36] since the scope of this thesis is on the experimental results. In this work, the support of the computational results in the analysis has made it possible, in particular, to propose the detailed atomic models for the studied surfaces and to elucidate the physical

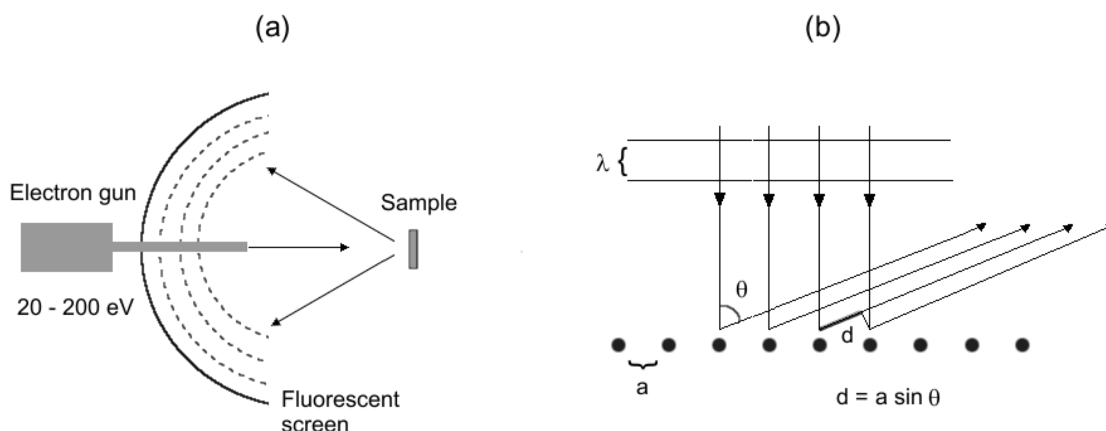

Figure 4. a) The experimental setup of LEED. b) Simple model for backscattering of electrons from a chain of atoms on a surface. De Broglie wavelength of electrons is λ, and the atomic spacing on a surface is a [43, 44].

mechanism behind the reconstructions.

3.1 Low energy electron diffraction (LEED)

LEED is the principal technique for determination of a surface structure. The sample is bombarded with beam of electrons of a well-defined low energy in the range 20 - 200 eV. Considering the wave particle duality, these electron waves are backscattered from the surface regions of high localised electron density, i.e. the surface atoms, which can be considered as point scatterers. The diffraction pattern of these backscattered electrons is detected on a fluorescent screen, and the experimental results are based on the analysis of the spots in the pattern. The experimental setup is schematically shown in Fig 4a [43, 44].

In order to detect a diffraction pattern, de Broglie wavelength of electrons $\lambda = h/p$ (h is Planck's constant and p is the electron momentum) has to be smaller than atomic spacing a on the surface. Since the momentum of an electron depends on its

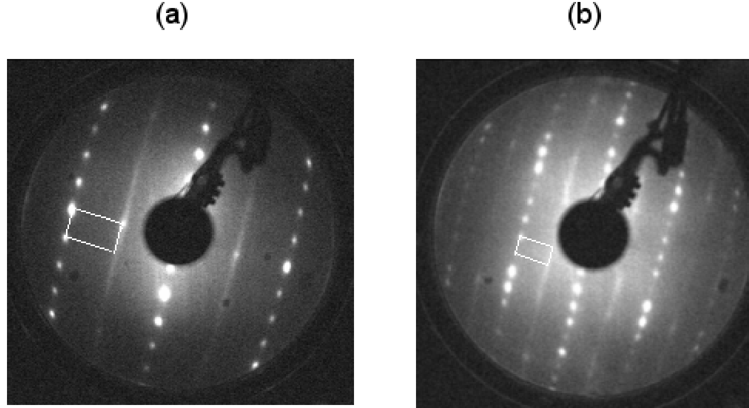

Figure 5. LEED images recorded with electron energies of 40 eV (a) and 120 eV (b). The white rectangles represent reciprocal lattice cells in real space. The images are recorded during the experiments from InAs(100)(2×4) surface.

kinetic energy eV, de Broglie wavelength is given by equation

$$\lambda = \frac{h}{\sqrt{2meV}}, \tag{1}$$

where m is electron mass, e is electronic charge and V is acceleration voltage. Figure 4b shows the paths of backscattered beams. The intensity of diffraction spots is significant only when the Bragg condition, $asin\theta = n\lambda$ (n is an integer), is fulfilled. According to the Bragg condition, the diffraction pattern is centrally symmetric ($\theta = 0$). Also, $sin\theta$ is inversely proportional to the lattice parameter a and to the root square of the acceleration voltage V. Considering this, the diffraction pattern shows the atomic geometry of the surface [43, 44]. The number of diffraction spots on the screen is controlled by the incident electron energy (eV). More specifically, the diffraction pattern is a direct picture of the reciprocal lattice of the surface. Examples of images from LEED experiments are shown in Fig. 5.

LEED is mostly used qualitatively, where the diffraction pattern is recorded and the analysis of the spot positions gives information on the size, symmetry and rotational alignment of the surface unit cell with respect to the substrate, or the (1×1) unit cell of an ideal, non-reconstructed surface. A quantitative LEED study is based on the measurement of the experimental intensity-voltage curves, which are

composed by following the intensity of a LEED spot as a function of the incident beam energy. These $I(V)$ curves are then compared to the theoretically calculated $I(V)$ curves from the surface structure on trial. In this thesis, only the qualitative application of LEED is used to determine the lattices of the studied surface layers [43].

3.2 Scanning tunneling microscopy (STM)

Since the first successful experiments by G. Binning, H. Rohrer and coworkers in 1981, STM has developed into an invaluable and probably the most powerful surface and interface analysis technique. STM provides images of the surface electronic density from which the atomic geometry can be determined by the correlation between the electronic and geometrical properties. The operation of STM itself does not require vacuum, but UHV system is required to avoid contamination of the surfaces of semiconductor samples. STM is based on a quantum mechanical phenomenon called tunneling, which has been known for more than eighty years. An electron, which can be described as a wave function, has a finite probability of entering or tunneling through a classically forbidden region, a potential barrier, which separates two classically allowed regions [45]. A conducting sample and a sharp metallic tip (for example a sharply etched tungsten wire), ideally only a single atom on the top, are brought within a distance of few tenths of a nanometer. This results in an overlap of the electronic wave functions. With an applied bias voltage, a tunneling current can flow from the occupied states of the sample to the unoccupied states of tip or vice versa, depending on the polarity of the sample. By using a piezoelectric drive system for the tip and a feedback loop, the surface topography can be obtained [45, 46].

The tunneling transmission probability for the electrons with energy E and applied bias voltage V is given by

$$T(E, eV) = \exp(-\frac{2Z\sqrt{2m}}{\hbar}\sqrt{\frac{\Phi_s + \Phi_t}{2} + \frac{eV}{2} - E}), \tag{2}$$

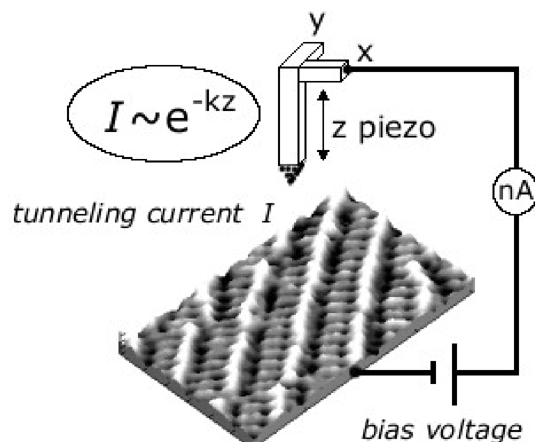

Figure 6. When the STM tip is close to the sample and a bias voltage is applied, electrons tunnel through a potential barrier between the STM tip and the sample, which creates a tunneling current I. Since the tunneling current depends exponentially of the tip-to-sample spacing Z (k is constant), even 0,1 nm differences in spacing can be recorded.

where $\Phi_{s,t}$ are work functions of the sample and the tip which describe the width of the potential barrier, m is the electron mass and Z is the tip-sample separation. Considering the tunneling transmission probability, for negative sample bias ($eV < 0$), the transmission probability is largest for $E = 0$, which correspond to the electrons at the Fermi level of the sample. Similarly, for positive sample bias ($eV > 0$), the transmission probability is largest for ($E = eV$) corresponding to the electrons at the Fermi level of the tip. For a typical work function of 3-4 eV, most of the tunneling current is within 0.3 V of the Fermi level, but also includes substitutional contributions below the Fermi level. Figure 6 shows the principle of operation of STM. Since the tunneling current depends exponentially on the distance Z, The decrease of the tip-to-sample spacing by only a tenth of a nanometer leads to a one order of magnitude increase in a tunneling current, which gives STM a high spatial resolution [46]. If the tunneling current is kept constant and the tip-sample separation is measured, an image of the electron density of a surface in the real space is obtained.

Nanoscale features can be imaged with the STM, but there are more information in the tunneling current than just the surface geometry. *Scanning tunneling spectroscopy* (STS) provides complementary information to the STM images, since by STS it is possible to measure the electronic density of states of the sample. By measuring the tunneling current as a function of the applied voltage *I(V)*, the electronic properties of the surface can be determined. However, the electronic density of states of the tip, and the voltage dependence of the tunneling current are unknown. The first issue can be overcome by measuring the tunneling spectra from a number of locations from the surface with the same tip, and since the density of states of the tip can be expected to be constant, it produces a constant background. Secondly, because the tunneling transmission probability does not vary rapidly near the band edges for semiconductor surfaces, the local density of states near the band edges can be reasonably understood by plotting only $\mathrm{d}I/\mathrm{d}V$ versus V [46].

3.2.1 Imaging the III-V(100) semiconductor surface

On III-V compound semiconductor surfaces, the group V elements are electronegative and the group III elements are electropositive. The electrons are highly localized, and the occupied states are around group V atoms and the unoccupied states are around group III atoms which means that by changing the polarity of the bias voltage, either occupied or unoccupied states can be imaged. On a large distance scale, STM measurements give useful information of the sample quality, the shape of step edges and overall surface morphology. Atomic resolution can be obtained both vertically and laterally under favourable conditions. It still has to be kept in mind that STM does not probe the surface atoms but gives an image of the electron density of a surface. Even though on a semiconductor surface the electrons are localized around specific atoms, the electron density does not necessarily give the exact atomic locations. STM is also subject to electrical or vibrational noise,

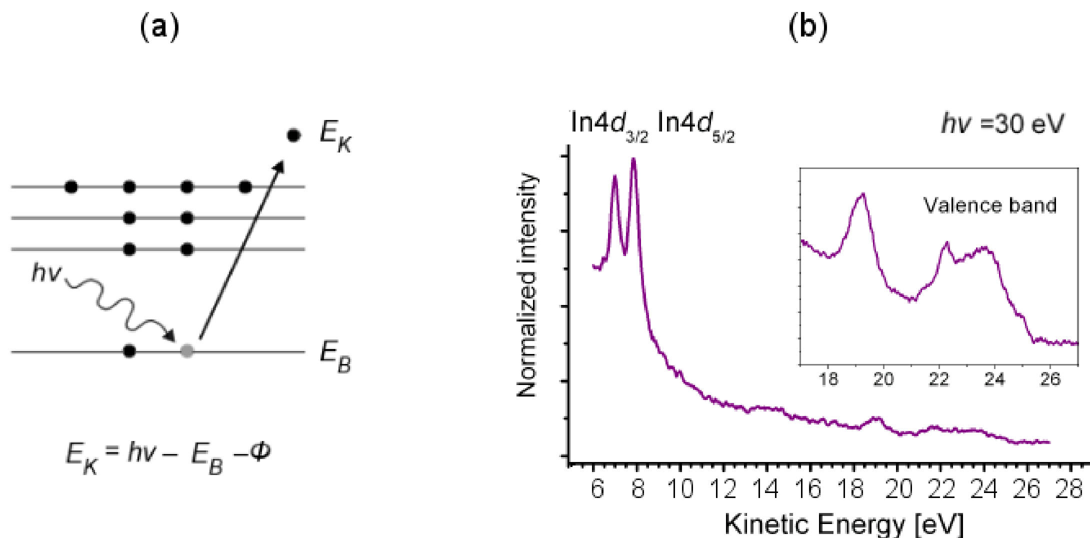

Figure 7. a) A schematic presentation of the photoelectric effect: An incoming photon with the energy $h\nu$ causes an emission of a photoelectron with kinetic energy E_K. E_B is the binding energy of the electron. b) Photoelectron spectrum measured from InAs semiconductor sample from the Fermi level (E_B = 0 eV) to the In 4d core levels (E_B = 16,9 eV and 17,7 eV). The inset is the magnified valence band spectrum.

and dull probes or multiple tips at the end of probe can create serious artifacts in the images. Often it is difficult to propose the detailed atomic structure on the basis of the measured images. This requires a careful analysis of the STM images, and a major advantage in this thesis is the possibility to compare the experimental images directly with the simulated ones for various energetically reasonable atomic models. Also, STM is more a local probe and it lacks the chemical identification of the elements. Therefore, it has been combined with other experimental techniques such as LEED and photoelectron spectrscopy.

3.3 Photoelectron spectroscopy

Photoelectron spectroscopy has been traditionally divided according to the radiation source. X-ray photoelectron spectroscopy (XPS) utilizes either Mg K_α or Al K_α radiation ($h\nu$ = 1253,9 eV, and $h\nu$ = 1486,6 eV, respectively). The technique was

first known as ESCA, Electron Spectroscopy for Chemical Analysis. XPS can be used to identify materials and determine their chemical composition, because each element has a unique set of binding energies [48]. The core-level electrons also conserve the individuality of the element and therefore core-level spectroscopy can be used to study the chemical and electronic state of the elements that exist within a material. Core-level electrons have higher binding energies compared to valence electrons, which participate in the chemical bonding [49]. The valence band is studied by UV-spectroscopy (UPS) using the radiation of the helium discharge lamp ($h\nu$ = 21.1 eV) [48, 49].

X-ray photoelectron spectroscopy was developed in the 1960s by Kai Siegbahn with his research group at the University of Uppsala, Sweden. Siegbahn received the Nobel Prize in 1981 to acknowledge his work. Photoelectron spectroscopy is based on the Einstein's photoelectric effect. When a sample surface is irradiated with photons of energy $h\nu$, electrons or *photoelectrons* are emitted from the sample as pictured schematically in Fig. 7a [48]. The photoelectrons are detected by an electron spectrometer according to their kinetic energy E_k, which is given by

$$E_k = h\nu - E_B - \phi, \tag{3}$$

where $h\nu$ is the energy of the incoming photon, E_B is the binding energy of the atomic orbital from which the electron originates, and ϕ is the work function of the spectrometer [48]. The photoelectron spectrum is plotted as a number of electrons detected (i.e. the emission intensity) versus the kinetic (or binding) energy of the detected electrons. The minimum energy needed to remove an electron from the solid into the vacuum is ϕ. An example of a plotted photoelectron spectrum measured from an InAs(100) sample is in Fig. 7b. The zero binding energy, which corresponds to the Fermi level, is defined as $h\nu$ - ϕ

The binding energy can be regarded as the energy difference between the initial and final states after the photoelectron has left the atom. Since there are a number

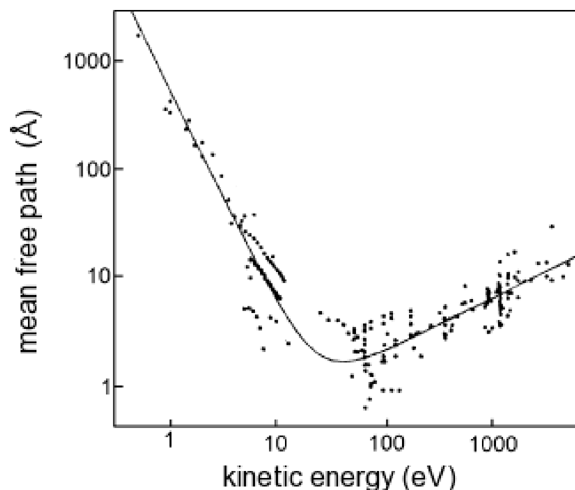

Figure 8. The inelastic mean free path of the electrons in solid. The dots represent measured data and the curve is theoretically calculated [51].

of possible final states of the ions of each type of atom, there is a variety of kinetic energies of the emitted electrons. There is also a different probability for each final state, which corresponds to the intensity of a photoelectron peak [48]. Since each element have atomic orbitals with different binding energies, each element produces a characteristic set of peaks in the spectrum. These characteristic peaks correspond to the electron configuration of the electrons within the atoms (e.g. 1s, 2s, 2p, 3s, etc.). The broadening of the peaks is due to several factors. The core-hole lifetime produces a Lorenzian contribution to the linewidth of the spectral line shape. The Lorenzian broadening increases for the deep core-levels since the core-hole lifetime becomes shorter [50]. The instrumental broadening is usually described by the Gaussian line shape, and is caused by the broadening due to the radiation source and the spectrometer. Variations in the elemental binding energies arise from different bonding environments of atoms or differences in the bonding environments of surface and bulk atoms [48]. The latter are called surface core-level shifts, which are discussed in more detail in section 3.3.2.

Even though the path length of the photons in the solid is of the order of mi-

crometers, the photo-emitted electrons that have escaped into the vacuum from the sample without losing their energy originates from only the surface layers [48]. The electrons which are emitted deeper than about few nanometers from the surface, have either lost part of their kinetic energy before escaping into the vacuum, or recaptured, or trapped in various exited states within the material. The so-called universal curve, presented in the Fig. 8, shows the inelastic mean free path of the electrons as a function of kinetic energy. The elastic photoelectron signal depth is about three times the mean free path. Thus, photoelectron spectroscopy is a surface sensitive technique and the escape depth depends on the kinetic energy of a photoelectron, meaning that the surface sensitivity can be varied if the kinetic energy of an electron can be varied [49].

3.3.1 Synchrotron radiation photoelectron spectroscopy

The X-rays and UV-radiation in conventional photoelectron spectroscopy have set energies. In order to change the photon energy and thus the kinetic energy of an electron to take full advantage of the photoelectron spectroscopy, synchrotron radiation is used. Synchrotron radiation is generated when an accelerated charged particle, for example an electron in a curved trajectory, emits radiation. In synchrotron radiation facilities, such as MAX-lab in Lund, Sweden, the radiation is produced by creating a magnetic field to force electrons in a curved trajectory in a storage ring. Storage ring is formed by bending magnets or insertion devices such as undulators or wigglers connected by straight sections. The radiation produced in this way has a characteristic polarization and it generates frequencies over a broad range of electromagnetic spectrum from microwaves to hard X-rays [52]. The relativistic electrons are injected into the ring from a linear accelerator, and various magnetic lenses keep the electrons traveling along the desired trajectory. The energy lost to the synchrotron radiation is replaced by a radiofrequency pulse which is generated

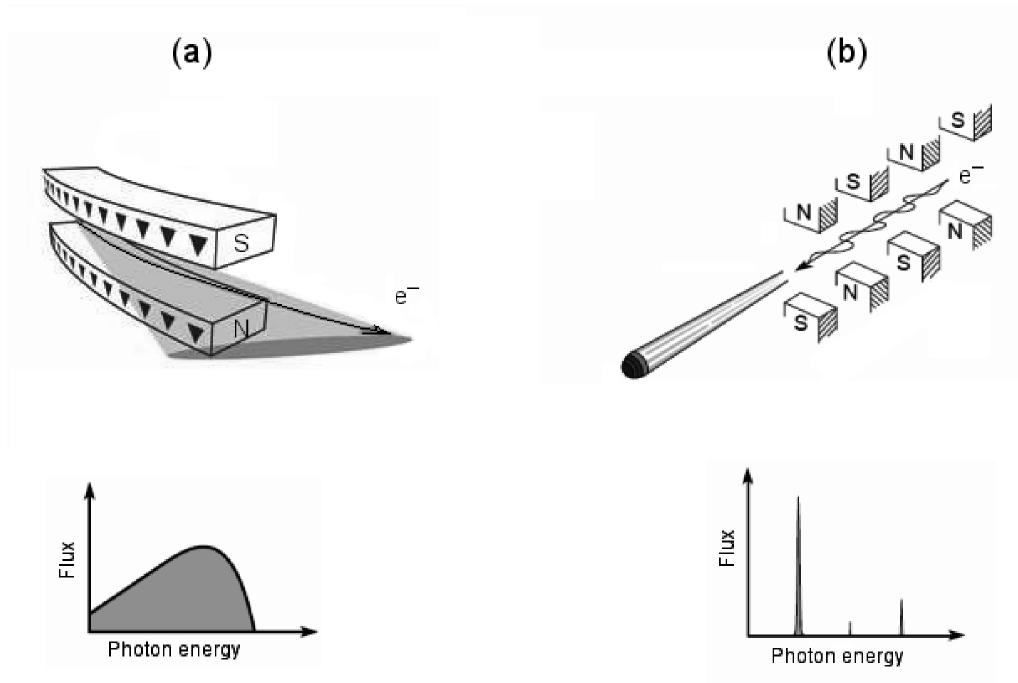

Figure 9. a) A bending magnet and the created radiation cone which is directed tangentially outward from the electron trajectory. The radiation spectrum is broad, and the emission angle wider and less bright than in the spectra from an undulator. b) A schematic image of the undulator radiation produced by a periodic magnetic field. The undulator spectra can be very narrow and extremely bright and may contain second or third order harmonics. Note that the two spectra are not scaled to each other. The images in the figure are modified versions of the images in ref. [52].

in a RF-cavity within the ring. The electron circulate the ring from a few hours to days depending on the ring. There are three types of magnetic structures typically used to produce synchrotron radiation: bending magnets, undulators and wigglers. Since the studies here have been made by using a bending magnet and an undulator based beamlines, they are briefly described here. Full technical information and theoretical approach of synchrotron radiation can be found in references [52, 53], for example.

Synchrotron radiation created by a bending magnet is illustrated in Fig. 9a. As the electros are bent from their straight path when passing through a uniform magnetic field, they emit X-rays tangentially to the plane of the electron beam. The synchrotron light from a bending magnet covers a wide and continuous spectrum, and is the least expensive method to produce synchrotron radiation, and thus more accessible than undulator based beamlines. An undulator, which is schematically drawn in Fig. 9b is a magnetic structure which is made up of an array of small magnets that force the electrons to follow an undulating, or wavy, trajectory. The radiation emitted at each consecutive bend overlaps and interferes with that from the other bends. This generates a much more focused, or brilliant, beam of radiation than that generated by a single magnet. Also, the characteristic emission angle is narrowed by a factor of $\sqrt{N}$, where N is the number of magnetic periods. In this research, beamline 41 at MAX I storage ring, and beamline I511-1 at MAX II in Lund, Sweden, were used in this research. Some supporting experiments were also carried out in ASTRID in Aarhus, Denmark. MAX I was build during the 1980's, and it is used both for producing synchrotron light and as an electron pulse stretcher for nuclear physic experiment. On the beamline 41, synchrotron light is produced by the dipole magnets. MAX II is a so-called third generation synchrotron source and was started 1996. Beamline I511 is an undulator based UV and soft X-ray beamline and the I511-1 experimental station is equipped with analyzers for XPS and X-ray

absorbtion spectroscopy on surfaces under UHV conditions.

3.3.2 The interpretation of the spectra

The analysis of the core-level spectra begins by fitting the spectra. The purpose of the spectral fitting is to decompose a spectrum into components. The fitting results include the number of separate components and their energy differences, which are called core-level shifts. The surface core-level shifts are determined as the difference in the binding energy of the electrons located at the sample surface and deeper in the bulk. A problem in the fitting is that the procedure is not unambiguous; there are several parameters included in the fitting, which are shortly reviewed in the following. The fitting approach described here has been used in several previous work and it has been found to produce reliable results (for example in Refs. [47, 54, 55]). Also, it is often useful to fit several spectra measured form the same sample with different photon energies and electron emission angles since the energy shifts should be independent form them. Naturally the uncertainty increases for small core-level shift components.

Firstly, the background is subtracted by Shirley's method [57]. The individual peaks are simulated with the Voigt function, which is a convolution of the Gaussian and Lorentzian functions. This is reasonable because the peak width is affected by both the Gaussian and Lorentzian broadenings [56]. The minimum number of components are introduced in the fitting. In the best case, the presence of separate components can be concluded from the peaks or shoulders in the spectrum. There are also several fitting parameters that can be fixed due to physical arguments. Spin-orbit splitting for different core-levels, which produces a doublet emission, are known. For example, the separation of the In $4d_{5/2}$ and In $4d_{3/2}$ components is 0.86 eV. The intensity ratio or the branching ratio of these peaks should be close to the statistical value of $(l+1)/l$, where l is the angular quantum number. $l = 2$ for the d orbitals, and

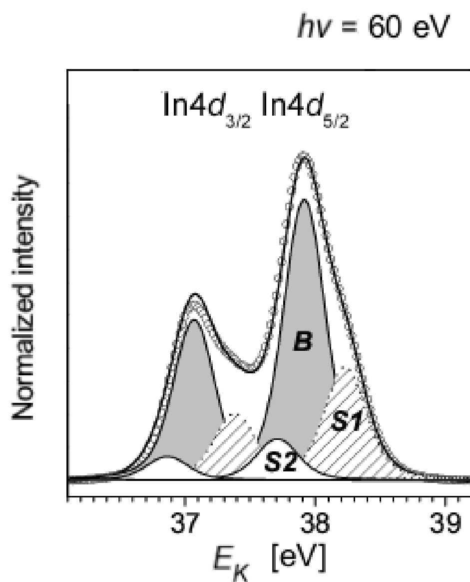

Figure 10. A fitted In $4d$ spectrum from the Bi-terminated InAs(100)surface taken with 60 eV photon energy. B corresponds to bulk emission and $S1$ and $S2$ are surface core-level shift components deducted by the fitting procedure.

thus the branching ratio is 1.5. Some variation can be allowed from the statistical value due to diffraction effects [58]. The Lorenzian widths are individual for different core-levels of different elements, and the Gaussian width is estimated according to the radiation source and the equipment used in the measurements. In some cases, it is possible to deduct the gaussian width from a spectrum, which can be fitted by only one component, and use this throughout the experiment. With the fitting method described above, the maximum peak width and different components in the spectrum are justified as well as possible, and the resulted largest energy separations between the components (core-level shifts) are obtained with good accuracy. An example of a fitted In $4d$ spectrum from the Bi-terminated InAs(100)surface is shown in Fig. 10. The number of core-level shifts and their intensity ratios elucidate the different atomic sites per unit cell. Moreover, the results should be compared to the simulated core-level shifts to resolve the atomic origins of each component in a spectrum. In this research, the experimental results were combined with theoretical calculations

by using the *ab initio* total energy program Vienna *ab initio* simulation package [36].

The valence band measurements are used to study the band structure or conductivity of the surface (or bulk). For a semiconductor sample, it is possible to determine the Fermi level position even if there are usually no electrons at the Fermi energy in a semiconductor. This problem can be circumvented by measuring the Fermi energy of a metal piece (e.g., clean Ta plate) which is in electrical contact with the sample. Because the Fermi level of the metal and the Fermi level of the sample are aligned, the Fermi level of the sample is also measured.

3.4 Sample preparation

The preparation of well-defined (crystalline) III-V surfaces is challenging but very relevant in making well justified conclusions from measurements. In particular, the core-level analysis requires uniform well-defined surfaces. The samples have to be prepared under UHV-conditions. It is not possible to remove amorphous natural oxides from the III-V substrate by only heating, since the substrate is decomposed at lower temperature than the surface oxides. Three methods to produce clean, oxide-free surfaces are used here. InAs(100) samples were mostly cleaned by Argon-ion sputtering and subsequent annealing. The sputtering destroys the crystal structure but the heating afterwards recovers the crystal into some extent. The second method is to use As-capping, which means that an amorphous As-layer is grown by MBE to protect the surface from oxidation while transferring the sample through air. The capping layer is removed once in UHV by heating the sample several hours around 300 °C. Naturally the best method is to use MBE equipment connected to the measuring chamber to grow samples *in Situ*. Such combination is rarely available but there is one at beamline 41 at MAX-laboratory. In order to evaluate the surface quality, the surfaces were characterized by LEED and STM. LEED is less sensitive to surface defects than STM but averages the whole sample surface. STM reveals

more localized defects. A smooth uniform surface is a result of a large number of sample-preparation experiments.

The cleaned samples were heated close to their decomposition temperature (depending on the sample, 450 °C – 600 °C) in order to get a well-defined group III-stabilized III-V(100) surface. Bismuth layer was deposited on the surface from a tungsten coil evaporator or an envelope-type evaporator at room temperature. The evaporation rate was initially calibrated with a quartz crystal microbalance to measure the film thickness. After the Bi deposition, the sample was heated gradually and the measurements were done after each heating step until no Bi was found on the surface. The parameters (i.e. the current through the tungsten filament, the evaporation time and the heating temperature) were optimized in order to produce reliable and moreover, repeatable experimental results.

4 Results and discussion

In order to interpret the behaviour and reconstruction of III-V(100) surfaces, and for the generalization of the established structural models it is important to gather detailed knowledge of the adsorption of group V elements on III-V(100) semiconductor surfaces. Reconstructions on clean III-V(100)surface have been widely studied. For other group V adsorbates besides As, the interest has mainly been focused on the behaviour of Sb on III-V(100) surfaces [23, 28], while Bi induced modifications on the surface structure of III-V(100) have gained only little attention earlier [42].

This section is an overview of the papers included in this thesis. The goal of this study was to investigate bismuth adsorption on several III-V(100) compound semiconductor surfaces. The experimental results are presented here, and this section is organized as follows: The section 4.1 describes the results of papers 1-3 which govern the properties of the Bi-induced III-V(100)(2×4) reconstruction commonly observed on several III-V(100) surfaces. Secondly, the section 4.2 considers the observations of peculiar Bi-stabilized III-V(100) surface structures (papers 4 and 5), which have not been seen previously on the III-V(100) surfaces. These findings are extremely important in determining the detailed physical properties behind the III-V reconstructions and the epitaxial growth of III-V materials for electronics. The last section is dedicated to explore the properties of Bi nanolines (papers 6 and 7). Thus, we found that in certain circumstances, Bi acts differently form other group V adsorbates on the III-V(100) surfaces, and the reasons why this happens and what might be the advantages of this kind of behaviour are discussed in the papers.

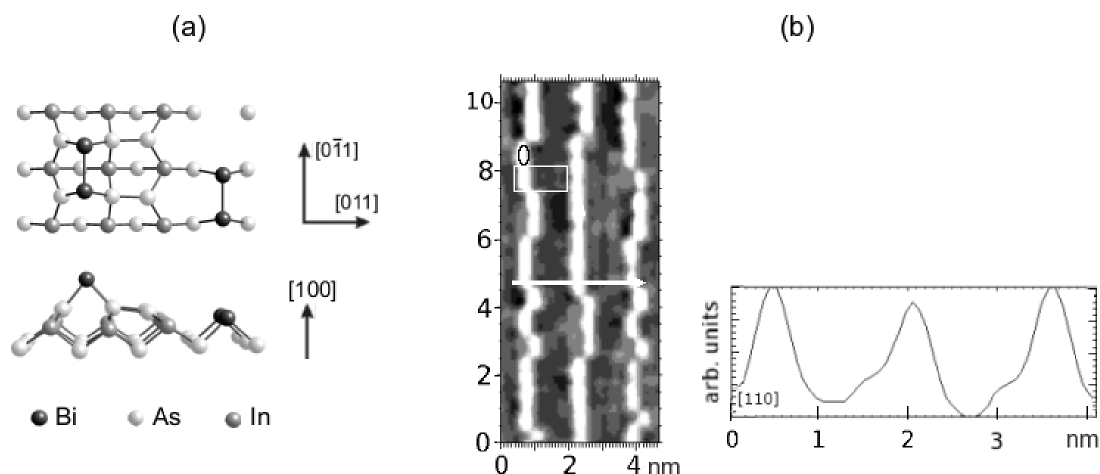

Figure 11. a) Top and side view of the so-called $\alpha2(2\times4)$ atomic structural model for the Bi/III-V(100) surface. b) Experimental STM image of the Bi/GaAs(100)(2×4) surface. A surface unit cell is marked with a white rectangle, and the black ellipse represents a surface dimer. The contour profile is measured along the white line in the STM image, and the bump before the peak in the line profile corresponds to the third layer group V dimer.

4.1 Bi-stabilized (2×4) reconstruction on III-V(100) semiconductor surfaces

Bi adsorption on GaAs(100), InAs(100) and GaInAs(100) were studied in the papers 1-3. Structural properties of Bi-induced reconstructions on these surfaces were studied by LEED, STM and photoelectron spectroscopy. After the Bi deposition, the samples were gradually heated and the changes in the reconstruction of the Bi/III-V(100) surface were monitored. With decreasing the Bi coverage by gradually heating the sample, (2×6), (2×8), (2×1), and (2×4) symmetries were deducted by LEED. A tentative atomic model was proposed for the Bi/InAs(100)(2×6) reconstruction according to the STM images and synchrotron radiation photoelectron spectroscopy, but the main focus was on the Bi/III-V(100)(2×4) surface, because the (2×4) reconstruction is common among III-V(100) substrates.

The reconstruction formed after the Bi deposition and heating at 320 °C - 400 °C (depending on the substrate) showed similar (2×4) symmetry as on the clean

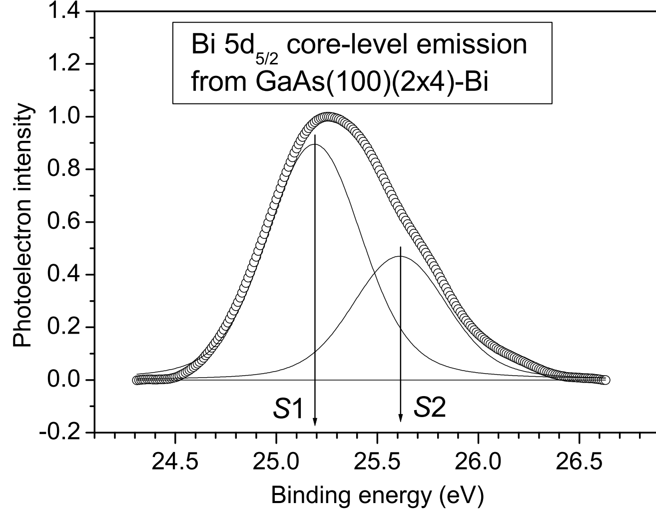

Figure 12. Bi $5d_{5/2}$ spectrum with two surface core-level shift components $S1$ and $S2$.

As-terminated III-V(100)(2×4) surface. According to the STM results, a III-V(100)-$\alpha 2$(2×4) model, which includes one group V dimer on the top layer and one group V dimer in the third layer, was proposed for the Bi/GaAs(100)-, Bi/InAs(100)- and Bi/GaInAs(100)(2×4) reconstruction. It is the same structural model which is experimentally observed and theoretically calculated to be energetically the most stable for the As-covered GaAs(100)- and InAs(100)(2×4) surface at a certain As-coverage [25, 47]. It is interesting that only the $\alpha 2$-structure was found on the Bi/III-V(100)(2×4) surface since on the other group V-stabilized III-V(100)(2×4) surfaces, $\beta 2$-structure (see Fig.3) is found to be dominant. A schematic image of this model and the experimental STM image and are presented in Fig 11.

Synchrotron radiation core-level spectroscopy was applied to the Bi/GaAs(100)- and Bi/InAs(100)(2×4) surfaces. The Bi $5d_{5/2}$ spectrum from the GaAs(100)(2×4) surface is presented in Fig. 12. Two different bonding sites are found for the Bi atoms on the surface at Bi coverage of 0.25 - 0.5 ML, which agrees well with the two different bonding environments in the $\alpha 2$ structure (Fig. 11a). The atomic

origins of these components were solved in Paper 5 by comparing the experimental and calculated core-level shifts. Namely, the high binding energy Bi component $S2$ arises from the topmost Bi atoms in the GaAs(100)(2×4)-$\alpha 2$ structure and the low binding energy component $S1$ arises from the third-layer Bi dimers. According to these results, Bi atoms occupy both the first and third layer sites on this surface.

4.2 Unusual (2×1) reconstruction on III-V(100) surface

Besides the common (2×4) reconstruction, a (2×1) reconstruction was found for Bi-stabilized III-V(100) surfaces with larger Bi coverage. [10, 59, 60]. Such a small unit cell, however, should not be stable on the III-V(100) surface according to the electron counting rule [21]. Therefore, it was very surprising that a well-ordered Bi-containing (2×1) reconstructions were found for several III-V substrates: GaAs, GaAsN, GaInAs, InAs, and InP. The unusual (2×1) reconstruction was investigated in papers 4 and 5. The experimental STM studies besides core-level and valence band photoemission results were compared with theoretical approach, and energetically favoured atomic models, both metallic and semiconducting, were proposed for the Bi-stabilized (2×1) reconstructions. Also, the fundamental questions, why both semiconducting and metallic Bi/III-V(2×1) structures are formed and what is the stabilizing mechanism behind them, are considered.

Figure 13 shows filled-state STM images from the Bi/GaAs(100)(2×1) surface and the $I(V)$ curves measured from the same areas of the sample by STS. Both images are measured from the similar sample(s). According to the $I(V)$ curves, both conducting and semiconducting areas are found. Also, by the valence band measurements, small Fermi-level photoelectron emission is found which means that the surface is at least partly metallic. Three atomic models for this (2×1) reconstruction are in Fig. 14. The model in Fig. 14a is labeled BiBi, and includes rows of Bi dimers paired in the $[0\bar{1}1]$ direction. This is the only atomic structure for this

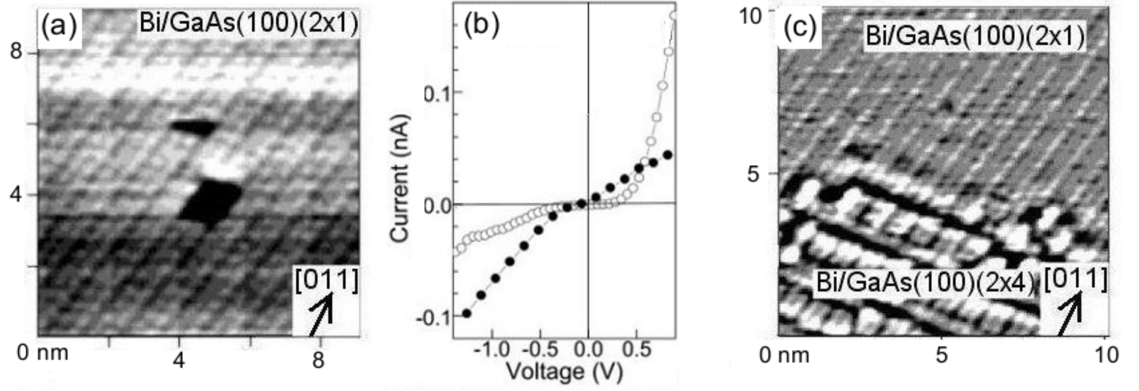

Figure 13. a) Filled-states STM image from the Bi-stabilized GaAs(100)(2×1) surface, and $I(V)$ curve [(b), solid circles] measured from the same location on the surface. c) STM image from the same (2×1) surface but different sample area, and $I(V)$ curve measured from it [(b), open circles]. Note that the same sample may contain different phases of the (2×1) reconstruction.

surface which is stable according to the theory. This is also metallic. By comparison of the calculated STM images with the measured ones it is concluded, that the STM image in Fig. 13a is measured from this GaAs(2×1)-BiBi reconstruction. However, the preparation conditions affect to the surface kinetics, which further affects to the reconstruction. Therefore, other possible phases besides BiBi are also considered. The STM image in Fig. 13c shows a different phase of which atomic model is in Fig. 14c. This is found to be semiconducting by STS with the energy gap of about 0.5 eV. It consists of mixed BiAs dimers in the topmost surface layer and includes Bi also in the second layer. The third phase for the (2×1) reconstruction (Fig. 14b) is identified from the STM images of the Bi/InP(100)(2×1) Fig. 14b. The theoretical diagram of the relative stabilities of (2×1) structure on Bi/GaAs is shown in Fig. 14 d.

The current understanding for the stabilizing mechanisms of the (2×1) structure, based on the ab initio calculations, is described in the following. First, the detailed geometry of the (2×1) reconstruction depends strongly on the chosen adsorbant and substrate. This is reflected clearly in the backbond angle (the angle

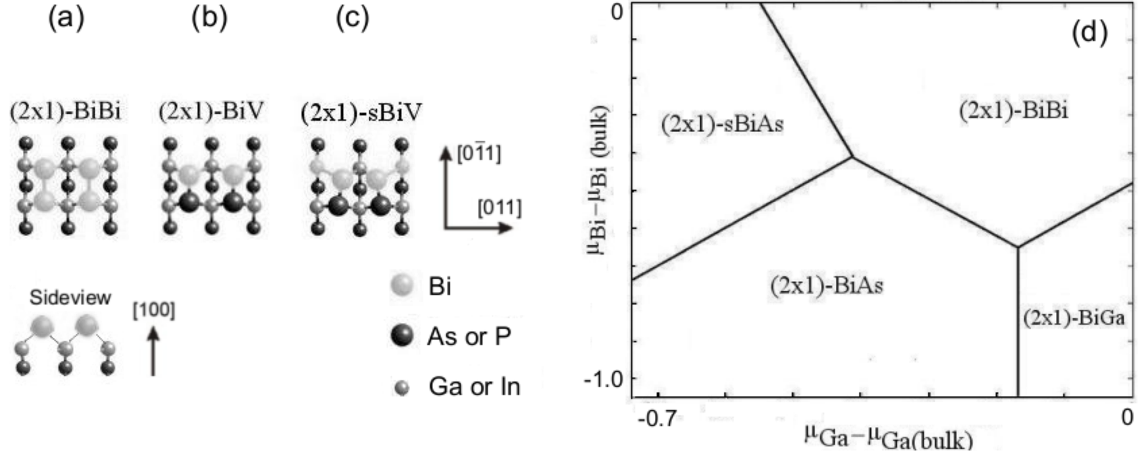

Figure 14. Metallic [(a) and (b)] and semiconducting (c) atomic models for the Bi-stabilized (2×1) reconstruction. d) Diagram of the energetically most favoured phases. (The model of the (2×1)-BiGa structure is not shown here).

between the bonds of dimer atoms and second layer atoms). For example, the backbond angle is 91.2° for Bi/GaAs(100)(2×1), whereas it is 105.7° for (hypothetical) GaAs(100)(2×1) structure. The repulsion between the dangling bond and the backbonds is decreased when the backbond angle is decreased from the ideal one of the bulk zincblende structure (109.5°). The backbond angle can be tuned by changing either the adsorbate or substrate. For example for the Bi/GaAs(100), the ratio of the lattice parameters of GaAs and GaBi determine the backbond angle in a reasonable accuracy. Based on the correlation explained above, it is suggested that when this ratio becomes smaller than 0.95° ±0.01° , the (2×1) reconstruction is stabilized. This condition also reflects the fact that the (2×1) reconstruction is not found on two-component (pure) III-V surfaces.

4.3 Formation of Bi nanolines on InAs(100) surface

Papers 6 and 7 show that by self-organization, on top of the Bi-stabilized InAs(100)(2×1) reconstruction, it is possible to produce a single-domain uniform array of Bi nanolines. This was also an intriguing observation since low-dimensional structures are

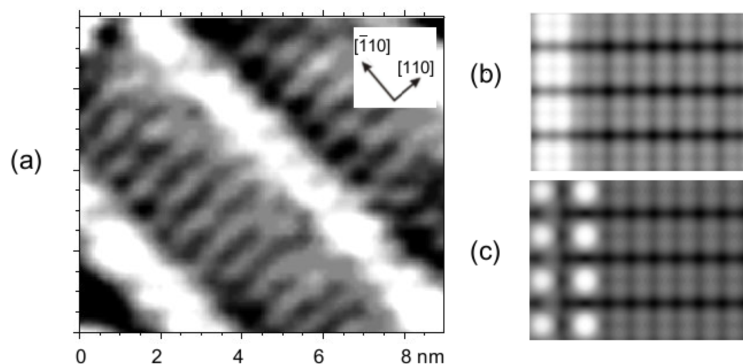

Figure 15. a) STM image from the Bi/InAs(100)-nanoline surface. b) and c) Two calculated STM images for two different atomic models for the same surface.

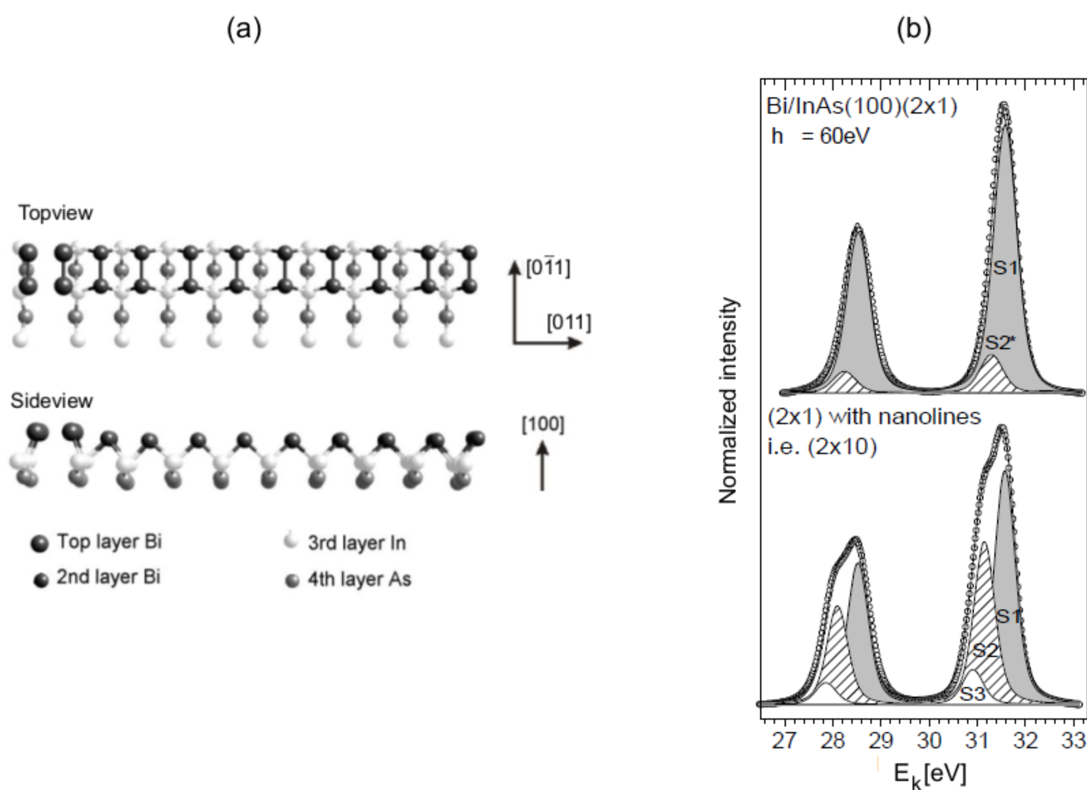

Figure 16. a) The suggested atomic structure for the Bi nanolines. b)Comparison of the Bi 5d core-level spectra from the Bi/InAs(100)(2×1) Surface and the Bi/InAs(100) nanoline surface.

being extensively explored due to their possibilities in future electronic devices and their apparently unique physical properties [14, 15]. Moreover, controlled growth of highly ordered single-domain structures over large sample areas has been proven to be difficult. The Bi nanolines are 4.3 nm apart, which is 10 times the lattice parameter ($a_0 = 4.3$ Å) of the InAs(100)(1×1) surface unit cell. This Bi/InAs(100)(2×10) surface is studied by LEED, STM and synchrotron radiation photoelectron spectroscopy. The experimental data were compared with the results of calculations considering a number of atomic models for this Bi nanoline surface. The energetically most favoured atomic structure was found with compatible experimental and theoretical STM images and surface core-level shifts.

Figure 15a shows an STM image measured from the Bi/InAs(100) sample surface. Two calculated STM images for two different atomic models, which were energetically the most stable structures for this surface are shown in Figs 15b and c. It is clear from these images that the calculated image in Fig. 15 b agrees better with the measured STM image. The atomic model for which the according theoretical STM image is calculated is presented in Fig. 16a. The nanolines are formed on top of the Bi/InAs(100)(2×1) reconstruction, which consists of BiBi dimer structure discussed in the last section. On top of these Bi dimers, the next Bi layer grows into one-dimensional Bi chains with Bi dimers parallel to the underlying dimers of the (2×1) structure. This corresponds to a Bi/InAs(100)(2×10) reconstruction. According to the calculations, the measured core-level shift components are assigned as follows: Bi dimers of the (2×1) structure ($S1$), the Bi dimers of the actual lines and the dimers on the side of the lines ($S2$), and dimers sitting next to the dimers on the side of the lines ($S3$). Also, the relative intensities of $S1$, $S2$ and $S3$ support the previous interpretation.

5 Conclusions

The III-V(100)(2×4) surface is the most important growth front in the epitaxial growth of III-V film layers for electronic and optoelectronic devices. In this thesis it has been shown that at certain bismuth coverage, Bi stabilizes a (2×4) reconstruction. The atomic structure of this reconstruction is similar to the previously found reconstructions on group V-stabilized III-V(100)(2×4) surfaces. However, the Bi-induced structure in the atomic scale consists of only a single phase, in which the surface unit cell contains one group V dimer in the topmost surface layer. This is in contradiction to the other group V-stabilized (2×4) surfaces, in which this so-called $\alpha 2$ structure has been found in a very narrow window of preparation conditions.

The second main finding of this work is the formation of well-ordered metallic Bi/III-V(100)(2×1) reconstruction. Also, a non-metallic (2×1) phase is found, which arises most likely from the crystal defects (i.e. antisites) below the surface. metallic Bi/III-V(100)(2×1) surface was tentatively predicted in Paper 6 to be a useful growth front for the epitaxial growth of III-V(100) films. Indeed, the recent experiments by Masnadi-Shirazi *et al.* proved the principle [12].

The third main result was the observation of a Bi-induced nanoline structure on InAs(100) surface. Such a large-scale one dimensional structure have not been previously found on III-V(100) semiconductor structure. The main reason to stabilize the nanolines was found to be the large atomic size of Bi. To recapitulate, at Bi coverage between 0.25 - 0.5 ML, the results of Bi adsorption on III-V(100) agree with those of other group V adsorbates. In contrast, at larger Bi coverages, the Bi/III-V(100) surfaces behave completely different form other group V stabilized III-V(100) surfaces.

References

[1] S. M. Sze, Semiconductor Devices, Physics and Technology, 2nd Edition, John Wiley & Sons 1985, 2002.

[2] S. Mokkapati and C. Jagadish, Materials Today 12 (2009) 22.

[3] M. R. Pillai, Seong-Soo Kim, S. T. Ho, and S. A. Barnett, Journal of Vacuum Science and Technology B 18 (2000) 1232.

[4] W. Huang, K. Oe, G. Feng, and M. Yoshimoto, Journal of Applied Physics 98 (2005) 98

[5] B. Fluegel, S. Francoeur, A. Mascarenhas, S. Tixier, E. C. Young, and T. Tiedje, Physical Review Letters 97 (2006) 067205.

[6] X. Lu, D. A. Beaton, R. B. Lewis, T. Tiedje, and M. B. Whitwick, Applied Physics Letters 92 (2008) 192110.

[7] S. Tixier, M. Adamcyk, T. Tiedje, S. Francoeur, A. Mascarenhas, Peng Wei, F. Schiettekatte, Applied Physics Letters 82 (2003) 2245.

[8] A. J. Ptak, R. France, C.-S. Jiang, and R. C. Reedy, Journal of Vacuum Science and Technology B 26 (2008) 1053

[9] Ph.Hofmann, Progress in Surface Science 81 (2006) 191.

[10] M. Ahola-Tuomi, P. Laukkanen, R. E. Perälä, M. Kuzmin, J. Pakarinen, I. J. Väyrynen, and M. Adell, Surface Science 600 (2006) 2349.

[11] P. Laukkanen, M. P. J. Punkkinen, H.-P. Komsa, M. Ahola-Tuomi, K. Kokko, M. Kuzmin, J. Adell, J. Sadowski, R. E. Perälä, M. Ropo, T. T. Rantala, I. J. Väyrynen, M. Pessa , L. Vitos, J. Kollár, S. Mirbt, and B. Johansson, Physical Review Letters 100 (2008) 086101.

[12] M. Masnadi-Shirazi, D. A. Beaton, R. B. Lewis, X. Lu, and T. Tiedje, J. Cryst. Growth 338 (2012) 80.

[13] F. J. Himpsel, K. N. Altmann, J. N. Crain, A. Kirakosian, J.-L. Lin,A. Liebsch, and V. P. Zhukov, Journal of Electron Spectroscopy and Related Phenomenon 126 (2002) 89.

[14] R. V. Belosludov, A. A. Farajian, H. Mizuseki, K. Miki, and Y. Kawazoe, Physical Review B 75 (2007) 113411.

[15] P. Segovia, D. Purdie, M. Hengsberger, Nature 402, 504 (1999).

[16] H.W. Yeom, Y. K. Kim, E.Y. Lee, K.-D. Ryang, and P.G. Kang, Phys. Rev. Lett. 95, 205504 (2005).

[17] W. Orellana, R. H. Miwa, Appl. Phys. Lett. 89, 093105 (2006).

[18] Friedhelm Bechstedt, Principles of Surface Physics, Springer-Verlag Berlin Heidelberg 2003.

[19] Robert F. Pierret, Semiconductor Fundamentals, 2nd Edition, Addison-Wesley Publishing Company 1988.

[20] Walter A. Harrison, Journal of Vacuum Science and Technology 16 (1979) 1492.

[21] M. D. Pashley, Physical Review B 40 (1989) 10481.

[22] Q-K. Xue, T. Hashizume and T. Sakurai, Progress in Surface Science 57 (1997) 1.

[23] Pekka Laukkanen, Atomic and electronic properties of GaAs(100) and InAs(100) semiconductor surfaces, Painosalama oy, Turun yliopisto 2005.

[24] Q-K. Xue, T. Hashizume, T. Sakurai, Applied Surface Science 141 (1999) 244.

[25] W. G. Schmidt, S. Mirbt, F.Bechstedt, Pysical Review B 62 (2000) 8087.

[26] W.G. Schmidt, Appl. Phys. A 75 (2002) 89.

[27] W.G. Schmidt and F. Bechstedt, Surface Science 409 (1998) 474.

[28] W.G. Schmidt and F. Bechstedt, Physical Review B 55 (1997) 13051

[29] A. Othake P. Kocán, J. Nakamura, A. Natori, N. Koguchi, Physical Review Letters 92 (2004) 236105.

[30] A. Ohtake, Physical Review B 74 (2006) 165322.

[31] R. H. Miwa and G. P. Srivastava, Physical Review B 62 (2000) 15778.

[32] A. Ohtake, M. Hirayama, J. Nakamura, and A. Natori, Physical Review B 80 (2009) 235329.

[33] Rolf. E. Hummel, Electronic properties of Materials, 3rd edition, Springer-Verlag USA 1985, 2001.

[34] D. M. Ceperley and B. J. Alder, Physical Review Letters 45 (1980) 566.

[35] J. P. Perdew and A. Zunger, Physical Review B 23 (1981) 5048.

[36] M. P. J. Punkkinen, P. Laukkanen, K. Kokko, M. Ropo, M. Ahola-Tuomi, I. J. Väyrynen, H.-P. Komsa, T. T. Rantala, M. Pessa, M. Kuzmin, L. Vitos, J. Kollár, and B. Johansson, Physical Review B 76 (2007) 115334.

[37] M. P. J. Punkkinen, P. Laukkanen, M. Ahola-Tuomi, J. Pakarinen, M. Kuzmin, A. Tukiainen, R. E. Perälä, J. Lång, M. Ropo, K. Kokko, L. Vitos, B. Johansson, M. Pessa, I. J. Väyrynen, Surface Science 603 (2009) 2664.

[38] L. J. Whitman, P. M. Thibado, S. C. Erwin,B. R. Bennett, and B. V. Shanabrook, Physical Review Letters 79 (1997) 693.

[39] G. P. Srivastava, Applied Surface Science 252 (2006) 7600.

[40] L. Li, B.-K Han, Q. Fu, and R.F. Hicks, Physical Review Letters, 82 (1999) 1879.

[41] W. G. Schmidt, P. H. Hahn, F. Bechstedt, N. Esser, P. Vogt, A. Wange, and W. Richter, Physical Review Letters, 90 (2003) 126101.

[42] P. Laukkanen, M. Ahola-Tuomi, J. Adell, M. Adell, K. Schulte, M. Kuzmin, M. P. J Punkkinen, J. Pakarinen, A. Tukiainen, R. E. Perälä, I. J. Väyrynen and M. Pessa, Surface science 601 (2007) 3395.

[43] D. J. O'Connor, B. A. Sexton, R. St. C. Smart (Eds.),

[44] http://www.chem.qmul.ac.uk/surfaces/scc/ Surface Analysis: Methods in Materials Science, Springer-Verlag, Germany 1992

[45] R. Wiesendanger, Scanning Probe Microscopy and Spectroscopy, Cambridge University Press 1994.

[46] H.-J. Güntherodt and R. Wiesendanger, Scanning Tunneling Microscopy I, Springer-Verlag, Germany 1992.

[47] P. Laukkanen, M. Kuzmin, R. E. Perälä, M. Ahola, S. Mattila, I. J. Väyrynen, J. Sadowski, J. Konttinen, T. Jouhti, C. S. Peng, M. Saarinen, M. Pessa, Phys. Rev. B 72 (2005) 045321.

[48] Handbook of X-ray Photoelectron spectroscopy, Perkin-Elmer Corporation 1992.

[49] C. R. Brundle, A. D. Baker, Electron Spectroscopy, Theory, Techniques and Applications vol 1, Academic Press Inc. 1977.

[50] J. C. Fuggle and S. Alvarado, Physical Review A, 22 (1980) 1615.

[51] M.P. Seah, W.A. Dench, Quantitative electron spectroscopy of surfaces: a standard data base for electron inelastic mean free paths in solids, Surface and Interface Analysis 1 (1979) 2.

[52] D. Attwood, Soft X-rays and extreme ultraviolet radiation, Cambridge University Press 1999.

[53] https://www.maxlab.lu.se

[54] C. McGinley, A. A. Cafolla, E. McLoughlin, B. Murphy, D. Teehan, P. Moriarty, D. A. Woolf, Appl. Surf. Sci. 158 (2000) 292.

[55] , G. Le Lay, D. Mao, A. Kahn, Y. Hwu, G. Margaritondo, Phys. Rev. B 43 (1991) 17.

[56] J. J. Joyce, M. Del Giudice, J. H. Weaver, J. Electron Spectrosc. Relat. Phenom. 49 (1989) 31.

[57] D. A. Shirley, Phys. Rev. B 5 (1972) 4709.

[58] H. W. Yeom, T. Abukawaa, Y. Takakuwaa, S. Fujimorib, T. Okaneb, Y. Oguraa, T. Miurab, S. Satob, A. Kakizakic and S. Konoa, Surf. Sci. 395, L236 (1998).

[59] P. Laukkanen, M. Ahola-Tuomi, M. Kuzmin, R. E. Perälä, I. J. Väyrynen, A. Tukiainen, J. Pakarinen, M. Saarinen, and M. Pessa, Applied Physics Letters 90 (2007) 082101.

[60] P. Laukkanen , J. Pakarinen, M. Ahola-Tuomi, M. Kuzmin, R. E. Perälä, I. J. Väyrynen, A. Tukiainen, J. Konttinen, V. Rimpiläinen, and M. Pessa, Physical Review B 74 (2006) 155302.

[61] M. Ahola-Tuomi, M.P.J. Punkkinen, P. Laukkanen, M. Kuzmin, J. Lång, K. Schulte, N. Räsänen, R.E. Perälä, and I.J. Väyrynen, Physical Review B 83 (2011) 245401.

[62] A. Z. AlZahrani and G. P. Srivastava, J. Appl. Phys. 106, 053713 (2009).

Original papers

Paper1

P. Laukkanen, **M. Ahola**, M. Kuzmin, R. E. Perälä and I. J. Väyrynen: *Bi-induced (2×6), (2×8) and (2×4) reconstructions on InAs(100) surface*, Surface Science Letters 598 (2005) L361.

©2005 Elsevier Science B. V.

Paper 2

M. Ahola-Tuomi, P. Laukkanen, R. E. Perälä, M. Kuzmin, J. Pakarinen, I. J. Väyrynen, and M. Adell: *Structural properties of Bi-terminated GaAs(001) surface*, Surface Science 600 (2006) 2349.

©2006 Elsevier Science B. V.

Paper 3

P. Laukkanen, **M. Ahola-Tuomi**, M. Kuzmin, R. E. Perälä, I. J. Väyrynen, A. Tukiainen, J. Pakarinen, M. Saarinen, and M. Pessa: *Structural properties of Bi-stabilized reconstructions of GaInAs(100) surface*, Applied Physics Letters 90 (2007) 082101.

©2007 American Institute of Physics.

Paper 4

P. Laukkanen, M. P. J. Punkkinen, H.-P. Komsa, **M. Ahola-Tuomi**, K. Kokko, M. Kuzmin, J. Adell, J. Sadowski, R. E. Perälä, M. Ropo, T. T. Rantala, I. J. Väyrynen, M. Pessa , L. Vitos, J. Kollár, S. Mirbt, and B. Johansson: *Anomalous bismuth-stabilized (2×1) reconstructions on GaAs(100) and InP(100) surfaces*, Physical Review Letters 100 (2008) 086101.

©2008 The American Physical Society.

Paper 5

M. P. J. Punkkinen, P. Laukkanen, H.-P. Komsa, **M. Ahola-Tuomi**, N. Räsänen, K. Kokko, M. Kuzmin, J. Adell, J. Sadowski, R.E. Perälä, M. Ropo, A. Tukiainen, T.T. Rantala, I.J. Väyrynen, M. Pessa, L. Vitos, J. Kollár, S. Mirbt, and B. Johansson: *Bismuth-stabilized (2×1) and (2×4) reconstructions on the III-V(100) surfaces: A combined first-principles and photoemission and scanning-tunneling-microscopy study*, Physical Review B 78 (2008) 195304.

©2008 The American Physical Society.

Paper 6

M. Ahola-Tuomi, P. Laukkanen, M. P. J. Punkkinen, M. Kuzmin, R. E. Perälä, I. J. Väyrynen, K. Schulte and M. Pessa: *Formation of an ordered pattern of Bi nanolines on InAs(100) by self-assembly*, Applied Physics Letters 92 (2008) 011926.

©2008 American Institute of Physics.

Paper 7

M. Ahola-Tuomi, M. P. J. Punkkinen, P. Laukkanen, M. Kuzmin, J. Lång, K. Schulte, N. Räsänen, R. E. Perälä, and I. J. Väyrynen: *Properties of self-assembled Bi nanolines on InAs(100) studied by core-level and valence-band photoemission and first-principles calculations*, Physical Review B 83 (2011) 245401.

©2011 The American Physical Society.